Published in "Nanomedicine 9(5): 607–621, 2014"
which should be cited to refer to this work.

Quantification of gold nanoparticle cell uptake under controlled biological conditions and adequate resolution

Aim: We examined cellular uptake mechanisms of fluorescently labeled polymer-coated gold nanoparticles (NPs) under different biological conditions by two quantitative, microscopic approaches. **Materials & methods:** Uptake mechanisms were evaluated using endocytotic inhibitors that were tested for specificity and cytotoxicity. Cellular uptake of gold NPs was analyzed either by laser scanning microscopy or transmission electron microscopy, and quantified by means of stereology using cells from the same experiment. **Results:** Optimal inhibitor conditions were only achieved with chlorpromazine (clathrin-mediated endocytosis) and methyl-β-cyclodextrin (caveolin-mediated endocytosis). A significant methyl-β-cyclodextrin-mediated inhibition (63–69%) and chlorpromazine-mediated increase (43–98%) of intracellular NPs was demonstrated with both imaging techniques, suggesting a predominant uptake via caveolin-medicated endocytois. Transmission electron microscopy imaging revealed more than 95% of NPs localized in intracellular vesicles and approximately 150-times more NP events/cell were detected than by laser scanning microscopy. **Conclusion:** We emphasize the importance of studying NP–cell interactions under controlled experimental conditions and at adequate microscopic resolution in combination with stereology.

Barbara Rothen-Rutishauser*[,1,2], Dagmar A Kuhn[1,3], Zulqurnain Ali[4], Michael Gasser[3], Faheem Amin[4], Wolfgang J Parak[4], Dimitri Vanhecke[1,3], Alke Fink[1], Peter Gehr[3] & Christina Brandenberger[3,5]

[1]Adolphe Merkle Institute, University of Fribourg, Marly, Switzerland
[2]Respiratory Medicine, Bern University Hospital, Bern, Switzerland
[3]Institute of Anatomy, University of Bern, Bern, Switzerland
[4]Fachbereich Physik & WZMW, Philipps Universität Marburg, Marburg, Germany
[5]Pathobiology & Diagnostic Investigation, Michigan State University, East Lansing, MI, USA
*Author for correspondence:
Tel.: +41 26 300 9502
barbara.rothen@unifr.ch

Keywords: electron microscopy • endocytosis inhibition • laser scanning microscopy • nanoparticle uptake • polymer-coated gold nanoparticle • stereology

In recent years, various types of nanoparticles (NPs; <100 nm in all three dimensions, ISO TS 27687:2008) have been designed for potential biomedical and pharmaceutical applications, such as vehicles for targeted drug delivery, nucleic acids, biomedical imaging or biosensing [1–3]. Therefore, an increasing number of research studies have focused on the interaction of NPs with biocellular systems [4,5]. To analyze different types of NP–cell interactions, such as cellular NP uptake, it is essential to have valuable techniques for visualization and quantification, which are mainly based on spectroscopy or microscopy [6].

The method of choice for the intracellular detection of NPs depends on the characteristics of the particles (fluorescence, size, and structure or electron density) and on the cellular structure of interest. Advantages of spectroscopy and different microscopic techniques have been reviewed in detail elsewhere [6,7]. In brief, spectroscopy such as inductively coupled plasma-mass spectroscopy [8] allows the quantification and detection of chemical NP elements within the cell, but does not provide any further information on the NP location within the cell. Fluorescence or laser scanning microscopy (LSM) allows real-time analysis or co-localization studies with fluorescently labeled structures [9]. Transmission electron microscopy (TEM) provides the highest resolution and allows quantification of NPs in subcellular structures [10].

However, sample preparation and NP quantification might be more labor intensive for TEM analysis and no real-time imaging can be performed. For this reason, many uptake studies use LSM to analyze the intracellular NP uptake and distribution [11,12]. Nevertheless, conventional LSM is limited in its spatial resolution by the optical diffraction limit and individual NPs cannot be resolved and quantified as single NPs if their mean distance is less than 200 nm.

In the current study we aimed to analyze cellular NP uptake by LSM and TEM. We therefore used gold (Au) NPs with a mean inorganic core diameter of 13 nm, coated with a polymer shell (isobutylene alt-maleic anhydride with 75% dodecylamine) and the red fluorescence marker ATTO 590 [9]. These NPs can easily be detected by TEM because of gold's high electron density and by LSM due to their fluorescent label. Furthermore, Au NPs have recently attracted a lot of interest concerning biological applications [13]. Au NPs are readily incorporated by many different types of cells and were found to be suitable in nanomedicine [13] since they show low toxicity [14,15], have convenient characteristics, like the potential to be coated with target molecules [16], and can be used in biomedical imaging [3]. Different *in vitro* and *in vivo* studies made use of similar sized Au NPs, which were coated with medical substrates such as drugs or DNA [17–19].

Additionally, we investigated the uptake mechanisms for Au NPs into human alveolar epithelial cells (A549). Cellular NP uptake mechanisms have already been the subject of many investigations, and there is convincing evidence that different endocytotic mechanisms are involved, such as phagocytosis, macropinocytosis, clathrin-mediated endocytosis, caveolae-mediated endocytosis, clathrin- and caveolin-independent endocytosis, and direct entering mechanisms summarized as adhesive interactions (reviewed in [20–22]). The different endocytotic pathways might be characteristic for specific cell types and further determine intracellular NP trafficking and fate [23]. It has been further shown that NP coatings induce specific endocytotic uptake mechanisms, either directly or via protein coating through interaction with their microenvironment [24,25].

To analyze the endocytotic uptake mechanism of Au NPs, specific inhibition of different pathways has been performed. Chlorpromazine hydrochloride is commonly used as an inhibitor of clathrin-mediated endocytosis, by leading to a loss of clathrin and the AP2 adaptor complex from the surface of the cell [26]. Furthermore, treatment of A549 cells with chlorpromazine was shown to specifically inhibit the uptake of the serum protein transferrin, which is known to enter the cells via clathrin-mediated endocytosis [27]. Fluorescently labeled transferrin was therefore used as a positive control to test for inhibitors of clathrin-mediated endocytosis. Caveolae and lipid raft internalization was shown to be inhibited by nystatin, filipin and methyl-β-cyclodextrin (mβcd) via alteration of the structure and function of the membrane [26]. Filipin and nystatin were described to be very specific without influencing clathrin-mediated endocytosis and macropinocytosis (reviewed in [26]). They have been tested in combination with choleratoxin subunit b (ctx-b) [28–30], which is known to enter the cells by caveolin-mediated endocytosis [30,31]. We therefore used fluorescent ctx-b as a control for inhibitors of caveolin-mediated endocytosis. Furthermore, the inhibitor dynasore was tested, which is known to interfere with both clathrin- and caveolin-mediated endocytosis. Dynasore is a cell-permeable, reversible, noncompetitive inhibitor of dynamin, which is required for clathrin- and caveolin-mediated endocytosis [26].

Since the endocytotic pathways used by particles varies between cells and most chemical inhibitors of endocytosis might lack specificity or cause adverse side effects, we first evaluated all inhibitors at different concentrations and incubation times in the presence of positive controls. The optimal conditions to inhibit caveolin- as well as clathrin-mediated endocytosis were then used to determine the intracellular number of Au NPs qualitatively as well as quantitatively by cutting-edge microscopy methods such as TEM and LSM combined with digital image restoration and stereology.

Materials & methods

Cell culture

Experiments were performed with the human alveolar epithelial type II cell line A549 obtained from American tissue Type Culture Collection. Cells were cultured in RPMI 1640 medium (GIBCO, Switzerland) and grown on six-well plates with cell-culture transwell inserts (BD Falcon, Germany), as described previously [15]. The cells were cultured for 7 days until they formed a confluent, tight layer and cell growth reached a plateau [32]. The medium was changed twice a week and exposures were performed on day 7.

NP synthesis & cell exposure

Hydrophobically capped Au NPs were synthesized as described previously [33]. The average NP size of the inorganic core was determined as 13.3 ± 0.5 nm by TEM (Figure 1A) and the concentration was measured by a UV/visible spectrometer (Agilent 8450) using an extinction coefficient of 4.62×10^8 $M^{-1}cm^{-1}$ at the plasmon peak of 526 nm. For transfer into aqueous solution the NPs were coated with an amphiphilic polymer. The synthesis of the amphiphilic polymer, poly(isobutylene-alt-maleic anhydride) (M_w ~6000 Da, Sigma #531278) with hydrophobic side chains, has

been described previously [34,35]. The fluorescent dye ATTO 590 was furthermore incorporated into the polymer shell. The number of fluorescent ATTO 590 dye molecules per NP in the final ATTO Au NP sample was estimated from the UV/visible absorption spectra (Figure 1B) by the respective absorption peaks of Au NPs and ATTO 590, as described previously [9,36]. A concentration of approximately 40 dye molecules per Au NP was measured. The fluorescence emission spectra of the NPs and the free ATTO 590 dye are shown in Figure 1C. A more detailed protocol about the synthesis and characterization of the particles is reported in the Supplementary Material (see online at www.futuremedicine.com/doi/suppl/10.2217/nnm.13.24).

Prior to exposure, NPs were diluted to a final concentration of 1.5 nM (9×10^{11} NPs/ml, as determined by UV/visible absorption spectroscopy) in RPMI without serum and vortexed and sonicated three times for 5 min. A volume of 500 µl NP suspension was applied per six-well insert and the cells were exposed for 1 h. All experiments were performed in triplicate with different cell passages. Cellular NP uptake, with and without inhibition of clathrin- or caveolin-mediated endocytosis, was analyzed by means of stereology after systematic random sampling on either LSM or TEM images.

Endocytosis inhibition

Different endocytotic inhibitors were tested for their efficiency, specificity and cell toxicity.

Clathrin-mediated endocytosis

Inhibition of clathrin-mediated endocytosis was tested with chlorpromazine hydrochloride (C8138, Sigma-Aldrich, Switzerland) used at final concentrations of 50 and 100 µM.

Caveolin-mediated endocytosis

Inhibition of caveolin-mediated endocytosis was tested with final concentrations of 25, 50 and 100 µM nystatin powder dissolved in tris (N6261, Sigma-Aldrich) and 50 µM nystatin suspension (N1638, Sigma-Aldrich) in sterile phosphate-buffered saline (PBS), 1 µg/ml filipin III from streptomyces filipinensis (F4767, Sigma-Aldrich) and 10 mM mβcd (C4555, Sigma-Aldrich).

Both mechanisms

Inhibition of both mechanisms was carried out with 40 and 80 µM dynasore monohydrate (D7693, Sigma-Aldrich).

Control experiments

Transferrin, coated with Alexa Fluor® 488 conjugate (T13342, Invitrogen, Switzerland), was used to test inhibition of clathrin-mediated endocytosis and ctx-b, labeled with Alexa Fluor 488 conjugate (C34775,

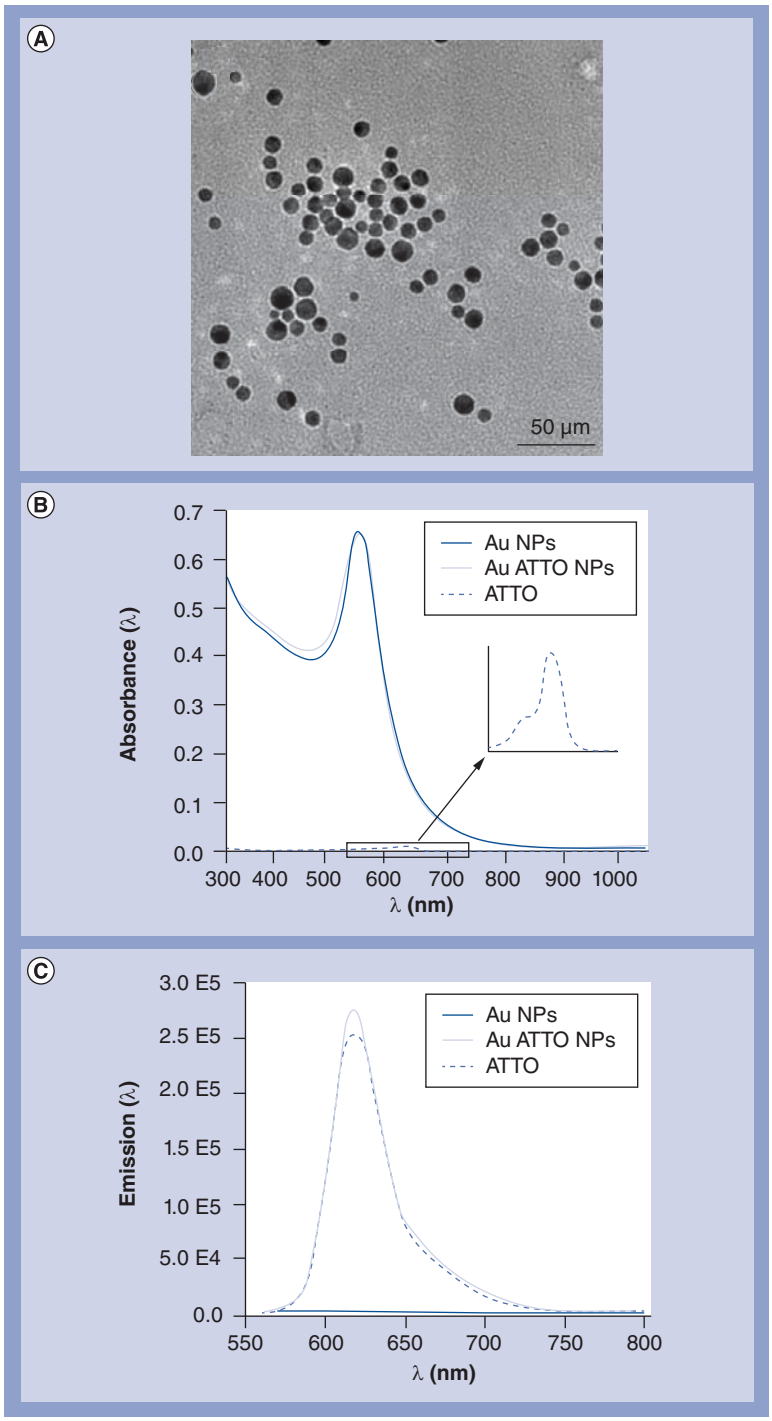

Figure 1. Characterization of gold nanoparticles. Polymer-coated Au NPs were characterized prior to use. A transmission electron microscopy image is shown in **(A)**. Note that only the inorganic gold core but not the organic surfactant shell provides contrast. The average gold core size is 13.3 ± 0.5 nm. **(B & C)** Absorbance spectrum and emission spectrum, respectively, of Au NPs with polymer shell with and without incorporated ATTO 590 dye, and of polymer micelles with ATTO 590. NP: Nanoparticle.

Invitrogen), was used to test inhibition of caveolin-mediated endocytosis. Transferrin was dissolved in dH_2O and 1% NaN_3 and diluted in RPMI cell culture medium without serum to a final concentration of 120 µg/ml. Ctx-b was dissolved in 10 mM PBS (pH 7.4) and 1% NaN_3 and diluted to a final concentration of 0.6 µg/ml PBS (pH 7.4) in RPMI prior to use.

Cell treatment

The cells were preincubated for 30 min with the inhibitors and further exposed to the endocytotic marker proteins either alone or in combination with the inhibitor (continuous inhibition). Exposures were carried out for 1 h. Inserts were cut into half and cells on one half were further processed and analyzed by means of LSM, as described below, and the other half for TEM.

Laser scanning microscopy

For LSM analysis, insert membranes with the cells were fixed with 3% paraformaldehyde (Sigma-Aldrich) and stained with either rhodamine phalloidin (red signal emission) or Alexa Fluor 633 phalloidin (far red signal emission; both Invitrogen) as described previously [15]. Analysis was performed with an inverted Zeiss LSM 510 Meta (Axiovert 200M, Zeiss, Switzerland) equipped with Argon/2 488 nm, HeNe 543 nm and HeNe 633 nm lasers. Image stacks were acquired with a 63× objective, twofold digital zoom and step size of 0.3 µm between z-stacks. Five different image stacks were randomly selected per insert membrane. In order to assure the randomness of the selected images and to give each area of the cell culture membrane an equal opportunity of being sampled, a random position outside of the cell culture membrane was determined, followed by a constant and defined x/y step movement and image acquisition at each randomly selected position on the cell membrane. See elsewhere for further details on unbiased, systematic random sampling [37]. After acquisition, scans were deconvolved by Huygens essential software (SVI, The Netherlands) to reverse the point spread function and increase the resolution of the images [38]. One could regard the maximum likelihood estimation-based deconvolution used in Huygens as a nonlinear (near) energy-conserving filter.

The 3D information such as the volume, surface or intracellular structures of the cells of the LSM images was further analyzed with Imaris software (Bitplane, Zürich). Therefore, location of marker proteins or NPs could be confirmed inside cells and intracellular NP events were counted manually in each test field (3D image stack with x/y area of 1600 µm² and height of cells). Intracellular particle events were counted according to the disector method [39]; a particle event was counted if present in a z-stack image, but missing in the consecutive one. Note that resolution of LSM is limited and therefore NP agglomerates might be detected as one single particle event. The average number of NP events per cell (NP_{Event}) was obtained by dividing the average intracellular NP events (N) per test field (A) with the mean cell number (C) per test fields (Equation 1). The average number of cells per test field was manually counted as well. Therefore, the x/y image border was used as an unbiased counting frame, including cells cut by the upper x-axes and the right y-axes and excluding cells cut by the lower x-axes and the left y-axes.

$$NP_{Event} = \frac{N/A}{C/A} \quad \text{(Equation 1)}$$

Transmission electron microscopy

The other half of the insert membrane with exposed cells was processed for TEM as described previously [15]. From the embedded cells, ultrathin sections were cut parallel to the vertical axis of the cells, mounted on copper grids and stained with lead citrate and uranyl acetate. Imaging was done at a magnification of 22,000× with a Morgani TEM (FEI Co Philips Electron Optics, Zürich, Switzerland). NP quantification was carried out by means of stereology as previously described [33]. Stereology is applied to estimate 3D structures, such as volume, surface, length or numbers from 2D images/sections. Here, the density of intracellular particles (N_V) was evaluated first and then multiplied with the average cell volume (V_C) to obtain the average number of NPs per cell (NP_{Cell}). Note that due to the better resolution of TEM compared with LSM individual NPs could be resolved and thus counted.

From every experiment, three random ultrathin TEM sections were screened by systematic uniform random sampling for intracellular NPs at a 2200× magnification. NPs were counted only if they occurred within a defined test field area (1.76 × 2.94 µm = 5.19 µm²) placed randomly over the cell images. The intracellular localization of each NP was further recorded to estimate the average intracellular NP distribution. The intracellular particle density (N_V) was obtained by dividing the number of intracellular NPs (N) in all test fields (n) to the total sampling volume (Equation 2). The total volume was estimated by multiplying the number of sampled test fields (n) with the test field area (A) and the section thickness (d). The section thickness was half of the diameter of the smallest fold, which was measured with TEM [40].

$$N_v = N/(n\,x\,A\,x\,d) \quad \text{(Equation 2)}$$

To estimate the mean cellular volume of the A549 cells, V_C, the vertical rotator [41] was used on semi-thin sections, which were stained with toluidine blue. Visualization and analysis was performed with a conventional light microscope coupled to a newCAST system (CAST 2.0, Olympus, Ballerup, Denmark) at an objective lens magnification of 600×. If a nucleolus was observed in an A549 cell, the cell was sampled for the cell volume estimation on vertical uniform random section by the nucleator, which can be used to estimate the volume from a 2D vertical uniform random section. The mean cell volume, V_C, was estimated for each experiment. The average number of NPs per cell, NP_{Cell}, was further obtained by using Equation 3:

$$NP_{Cell} = N_V \times V_C \quad \text{(Equation 3)}$$

Note that effects of uneven cellular shrinkage during processing of TEM and LSM samples were considered as irrelevant for comparison on intracellular particle number, since the cellular reference volume was established separately for TEM and LSM samples post-preparation to avoid any conflict of shrinkage between the two techniques. For further readings on the effect of tissue shrinkage and particle counts we refer the reader elsewhere [42].

Lactate dehydrogenase assay

In each experiment, 1 ml of the supernatant was sampled for the lactate dehydrogenase (LDH) assay to determine cytotoxicity [43]. Briefly, Triton X (2% in RPMI, 30 min preincubation) was used for cell lysis and the positive control. The supernatant of untreated cell was used as the negative control. The LDH assay was performed with the Cytotoxicity Detection Kit (Roche Applied Science, Germany) according to the supplier's manual. Each supernatant was measured in triplicates.

Statistics

To investigate the significance ($p < 0.05$) of the LSM and TEM results, the Sigma Stat program for Windows (Version 3.10, Systat Software, Inc., Richmond, CA, USA) was used. With one-way analysis of variance, pairwise multiple comparison procedure (Student-Newman-Keuls) was tested. Results are presented as mean (n = 3) ± standard error of the mean.

Results

A549 cells were grown for 7 days on a membrane insert as described [32]. Under these conditions, the cell number doubles and then levels off within 5 days in culture, which is important in order to provide the fully functional properties of epithelial cells [44].

Endocytotic inhibitors

Different inhibitors of clathrin- and caveolin-mediated endocytosis were tested for their specificity and cell toxicity. Fluorescently labeled transferrin, which was shown to enter the cells by clathrin-mediated endocytosis [45], and fluorescently labeled ctx-b, which enters via caveolin-mediated endocytosis [46], were used to test efficiency and specificity of the inhibitors (Figure 2). Cell viability was analyzed either morphologically by LSM and TEM (Figure 3) or by the LDH assay. The results of all inhibition experiments are summarized in Table 1 and the results of the LDH assay are shown in Table 2.

Optimal inhibition of clathrin-mediated endocytosis, which was tested with fluorescently labeled transferrin and analyzed by LSM, was achieved by 50 and 100 µM chlorpromazine (Figure 2A). Chlorpromazine was shown to be very specific in inhibiting uptake of transferrin but not ctx-b (Figure 2E) and did not affect the cells, even when the concentration or incubation time was increased.

Caveolin-mediated endocytosis was best inhibited by 10 mM mβcd (Figure 2D). However, although it is generally stated that mβcd inhibits both caveolin- as well as clathrin-mediated endocytosis [47], clathrin-mediated endocytosis was observed when the cells were exposed to mβcd since only partially inhibited transferrin uptake was seen (Figure 2B). Furthermore, cells could only be exposed to mβcd for a limited time period (30 min preincubation) since the cell morphology and epithelial integrity were affected by prolonged exposure for 90 min. Exposure times were therefore limited to 30 min before addition of NPs. Caveolin-mediated endocytosis was only successfully inhibited by mβcd, since nystatin, neither as a powder dissolved in tris buffer nor in suspension directly received from the supplier, was capable of inhibiting cellular ctx-b uptake via caveolin-mediated endocytosis, even when the inhibitor concentration or incubation time was increased. Filipin, another potential inhibitor of caveolin-mediated endocytosis, did not inhibit the uptake of ctx-b, but the cell morphology and epithelial integrity was negatively affected (Figure 2F).

The inhibitor dynasore, which is known to interfere with both clathrin- as well as caveolin-mediated endocytosis via reversible and noncompetitive inhibition of dynamin, was not effective at an exposure time of 30 min even at increased concentrations (Figure 2C). However, at prolonged exposure times, the inhibitor led to a strong auto-fluorescent cell signal associated with a loss of cell viability.

In addition, morphological analysis of cells treated with and without endocytotic inhibitors was assessed

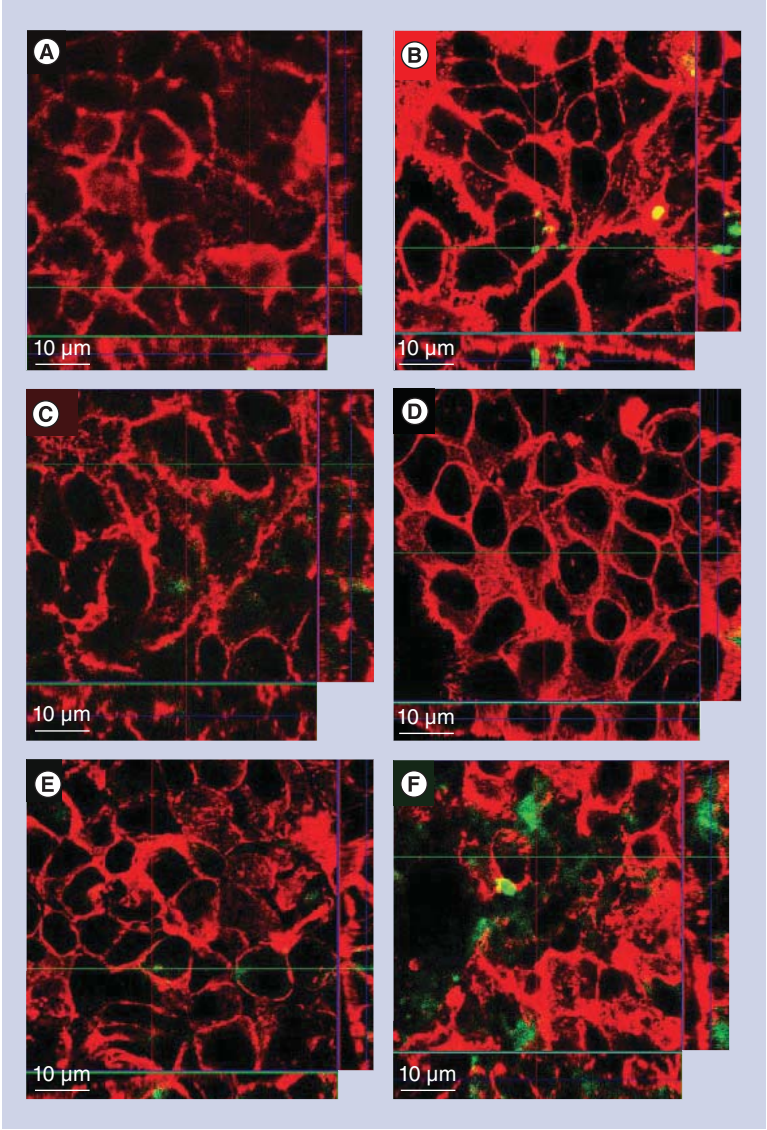

Figure 2. Inhibitor specificity and efficiency of clathrin- and caveolin-mediated endocytosis. (A–C) Clathrin-mediated endocytosis was tested with fluorescent transferrin (green) uptake into the cells (red cytoskeleton) within 1 h of exposure time. **(A)** A 30-min preincubation with 100 µM chlorpromazine was shown to inhibit clathrin-mediated endocytosis, whereas a 30-min preincubation with **(B)** 10 mM methyl-β-cyclodextrin or **(C)** 80 µM dynasore did not. Caveolin-mediated endocytosis was tested with fluorescent choleratoxin subunit b (green) uptake within 1 h of exposure time as shown in figures **(D–F)**. **(D)** A 30-min preincubation with 10 mM methyl-β-cyclodextrin successfully inhibited choleratoxin subunit b uptake, but preincubation with **(E)** 100 µM chlorpromazine or **(F)** 100 µM filipin did not result in inhibition of caveolin-mediated endocytosis.

by LSM and TEM, revealing that the morphology as well as the actin cytoskeleton was not impaired in the presence of the inhibitors (Figure 3).

Cellular NP uptake

The cells were exposed to a final concentration of 1.5 nM Au NPs for 1 h after preincubation with the optimal endocytotic inhibitors (chlorpromazine, mβcd or none). Intracellular NPs were further visualized by either LSM or TEM and quantified by stereological approaches as described in the 'Materials & methods' section.

NP uptake evaluation by LSM

Visualization of intracellular NPs in A549 cells by LSM with or without inhibitors and their quantitative evaluation are shown in Figure 4. The NPs could be detected inside A549 cells as NP events (control without inhibitor; Figure 4A), whereby one NP event refers to one individual spot of fluorescence, which likely corresponds to an NP-filled vesicle as previously shown for other fluorescent NPs [48]. As shown in Figure 4B, chlorpromazine did not inhibit NP uptake and intracellular NP events were still detected. Almost no intracellular NPs were seen in the presence of mβcd and NPs were mostly attached to the outer cell membrane (Figure 4C). Next, we counted the intracellular NP events, resulting in 42.2 ± 13.4 NP events/cell for noninhibited cells (control), 60.8 ± 11.4 for chlorpromazine-treated cells and 13.1 ± 3.8 for mβcd-treated cells (Figure 4D). Hence, cells treated with mβcd showed a 69% inhibition of NP uptake compared with untreated controls, whereas treatment with chlorpromazine surprisingly resulted in a 43% increase in NP uptake. However, a significant difference ($p = 0.042$) of intracellular NP events was measured between mβcd- and chlorpromazine-treated cells, but not between treated and untreated control cells.

NP uptake evaluation by TEM

The evaluation of intracellular NP numbers by TEM resulted in the total number of NPs, since TEM, in comparison to LSM, allows the resolution and detection of single particles. Intracellular NPs as detected by TEM and the average cellular NP numbers are shown in Figure 5. In the TEM images (Figures 5A–C) we could confirm that NPs were localized in vesicles of different sizes, which indicates endocytotic NP uptake. The number of NPs taken up per cells was 5365 ± 779 for noninhibited cells, 10612 ± 1169 for chlorpromazine-treated cells and 1992 ± 788 for mβcd-treated cells (Figure 5D). Hence a significant difference ($p < 0.05$) in the numbers of intracellular NPs between control and chlorpromazine- or mβcd-treated cells was measured as well as between chlorpromazine- and mβcd-treated cells. The number of mean intracellular NPs was twice as high in the cells treated with chlorpromazine and a 63% decrease was seen in mβcd-treated cells compared with the positive control. Therefore, the

trends observed by TEM and LSM were similar, but only by TEM is it possible to evaluate the total NP number. The results suggest that a detected fluorescent signal covers on average a cluster of 150 NPs.

The intracellular localization of the NPs was further evaluated and it was shown that 95% or more of the NPs were located in intracellular vesicles (Figure 6). The remaining intracellular NPs were detected free in the cytosol and no particles were found in any other cellular organelles such as the mitochondria, nucleus or endoplasmic reticulum. These results show that endocytosis is the foremost method of cellular NP internalization. The inhibition of different endocytotic pathways did not result in a difference in cellular NP localization (% NPs in vesicle: control 94.9 ± 3.1, chlorpromazine inhibition 99.8 ± 0.1, mβcd inhibition 98.6 ± 1.0).

Discussion

The great potential of nanosized particles such as Au NPs for diagnostic and therapeutic applications requires a thorough understanding on how these NPs interact with cells and how they are taken up, and their subsequent detection and localization within cells is of central importance [49]. Once intracellular NPs are identified, their distribution in different cellular compartments, such as endosomes, lysosomes, mitochondria, the nucleus or cytosol, may also provide some indications as to a potential diagnostic or drug delivery system. By using well-defined and characterized fluorescently labeled polymer-coated Au NPs, two different quantitative microscopy methods could be directly compared: the fluorophore was analyzed by LSM and the electron dense Au core by TEM. These two methods were then applied to reveal the uptake mechanism using lung cells *in vitro* with inhibitors for various endocytotic uptake pathways.

Efficient inhibition of clathrin- & caveolin-mediated endocytosis

Various studies have been performed using chemical inhibitors of endocytosis to analyze uptake mechanisms of NPs into cells [12,50,51]. However, efficiency of inhibitors might vary within cell types and depends on exposure concentration and time. It has, for instance, been shown that the same NP type can explore different uptake mechanisms to enter different cell types [50]. In addition, inhibitors can induce cytotoxicity at higher concentrations. We therefore carefully analyzed commonly used inhibitors of endocytotic pathways. In A549 cells, we found that efficient inhibition of clathrin-mediated endocytosis was only achieved with 100 µM chlorpromazine and caveolin-mediated endocytosis with 10 mM mβcd (30 min preincubation, Table 1). Although mβcd partially inhibited clathrin-mediated transferrin uptake, as shown previously [47], this inhibitor was most specific in the inhibition of caveolin-mediated ctx-b uptake compared with the other inhibitors tested (Table 1). Cell viability was not affected by these two inhibitors at the used incubation times and concentrations. The lowest effective concentration of inhibitors was always chosen for the exposures to reduce possible cell damage. The other tested inhibitors were either less specific or damaged the cells. If not suitable for further exposure with NPs, some

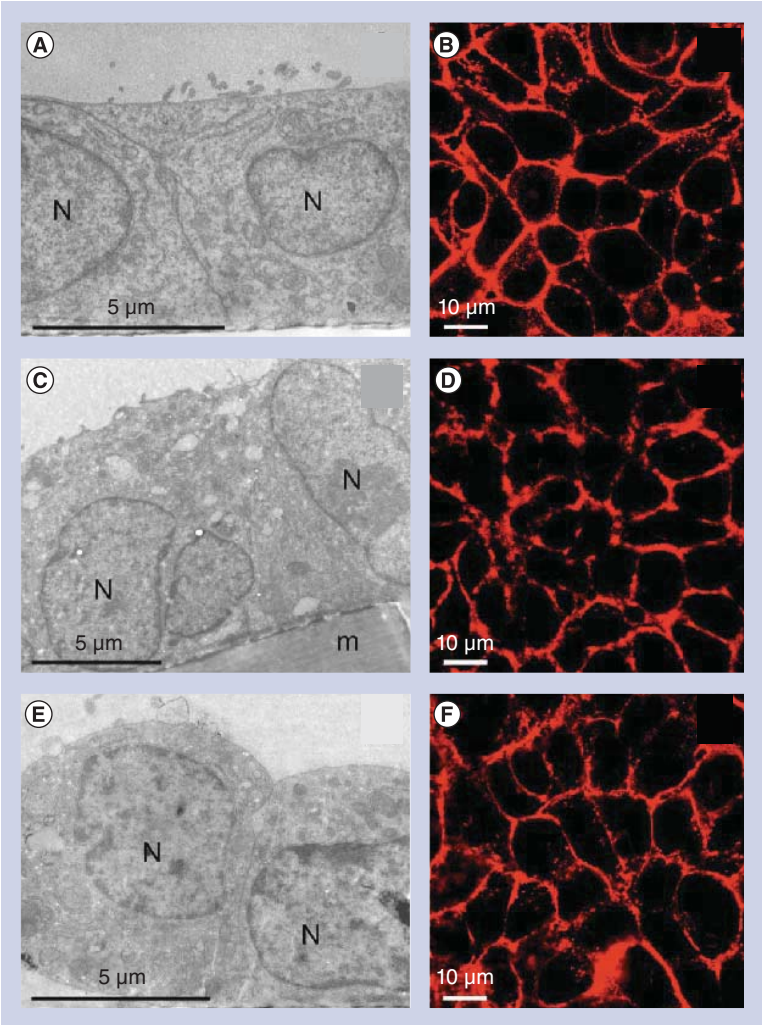

Figure 3. Morphological analysis of cells treated with and without endocytotic inhibitors. Cellular morphology of untreated control cells and cells exposed to endocytotic inhibitors at optimal inhibition conditions were compared by **(A C & E)** transmission electron microscopy and **(B, D & F)** laser scanning microscopy. Control cells without inhibitor treatment are shown in **(A & B)**, cells treated with 100 µM chlorpromazine for 30 min in **(C & D)** and cells treated with 10 mM methyl-β-cyclodextrin for 30 min in **(E & F)**. Cells of both inhibitor conditions appeared healthy and viable, comparable to control cells. Red stain: cytoskeleton. m: Cell culture membrane; N: Nuclei.

Table 1. Analysis of specificity and efficiency of the different endocytotic inhibitors.			
Inhibition of clathrin-mediated endocytosis			
Inhibitor exposure	**Inhibition-positive control (transferrin)**	**Inhibition-negative control (ctx-b)**	**Cell viability**
Chlorpromazine 100 µM 30 min	Inhibition	No inhibition	Good
Chlorpromazine 100 µM 90 min	Inhibition	No inhibition	Good
Inhibition of caveolin-mediated endocytosis			
Inhibitor exposure	**Inhibition-positive control (ctx-b)**	**Inhibition-negative control (transferrin)**	**Cell viability**
Nystatin 100 µM 30 min	No inhibition	Not tested	Good
Nystatin 100 µM 90 min	No inhibition	Not tested	Good
Filipin 100 µM 30 min	No inhibition	Not tested	Impaired
Filipin 100 µM 90 min	No inhibition	Not tested	Impaired
mβcd 10 mM 30 min	Inhibition	Slight inhibition	Good
mβcd 10 mM 90 min	Inhibition	Inhibition	Impaired
Inhibition of dynamin-dependent endocytosis			
Inhibitor exposure	**Inhibition-positive control (transferrin)**	**Inhibition-positive control (ctx-b)**	**Cell viability**
Dynasore 40 µM 30 min	No inhibition	No inhibition	Good
Dynasore 40 µM 90 min	No inhibition	Not tested	Good
Dynasore 80 µM 30 min	No inhibition	Not tested	Impaired
Dynasore 80 µM 90 min	Inhibition	Slight inhibition	Impaired

Different common endocytotic inhibitors were tested for specificity, efficiency and cell impairment at various concentrations and exposure times. Fluorescently labeled proteins, such as transferrin and ctx-b, were used to test the grade of inhibition. Transferrin was used as a marker for clathrin-mediated endocytosis and ctx-b for caveolin-mediated endocytosis. Impaired cells showed signs of membrane disruption, loss of integrity and loss viability as detected by a strong signal of autofluorescence.
ctx-b: Choleratoxin subunit b; mβcd: Methyl-β-cyclodextrin.

inhibitors and marker proteins were not checked in the pre-experiments (Table 1). Dynasore was previously described to inhibit caveolin-mediated uptake of ctx-b in human osteosarcoma cell lines at a concentration of 80 µM following preincubation for 30 or 60 min [52]. In our study, dynasore only showed inhibition when used at higher concentrations and the inhibition was prominent for transferrin uptake as well as for ctx-b uptake [26,53]. Nevertheless, dynasore was not optimal because of adverse effects such as impairment of cell viability. The inhibitor filipin was shown to inhibit ctx-b uptake by 58% in CaCo-2 human intestinal epithelial cells [28], as well as in A549 cells at a concentration of 1 µg/ml with a preincubation time of 30 min [27]. A reduction of caveolin-mediated transcellular transport of albumin was also shown by filipin [54]. However, in the current study, no efficient inhibition of caveolin-mediated endocytosis could be achieved by this inhibitor, although similar conditions were used. It can be assumed that the instability of the inhibitor [55] might be responsible for the lack of inhibition over time. Since no inhibition in the uptake of ctx-b was achieved but cellular damage occurred, filipin was not considered as an optimal inhibitor for our study. Nystatin, in tris or in suspension, did not show any inhibition, even at high concentrations. It has been suggested that this inhibitor is used in combination with the hormone progesterone for increased efficiency [56].

Table 2. Cell viability of particle- and inhibitor-exposed cells.	
Cell	**OD**
Untreated cells (negative control)	1.33 ± 0.25
Lysed cells (positive control)	1.61 ± 0.25
Cells + 1.5 nM NP	1.32 ± 0.17
Cells + 1.5 nM NP + 100 µM chlorpromazine	1.21 ± 0.19
Cells + 1.5 nM NP + 10 mM mβcd	1.07 ± 0.11

Cell viability was measured with the lactate dehydrogenase assay in control cells and cells treated with inhibitors of endocytosis for 30 min and exposed to NPs for 1 h. Results are presented as the mean OD of an n = 3 ± standard error of the mean.
mβcd: Methyl-β-cyclodextrin; NP: Nanoparticle; OD: Optical density.

Cellular NP uptake

It was shown that more than 95% of the intracellular Au NPs imaged by TEM were detected within

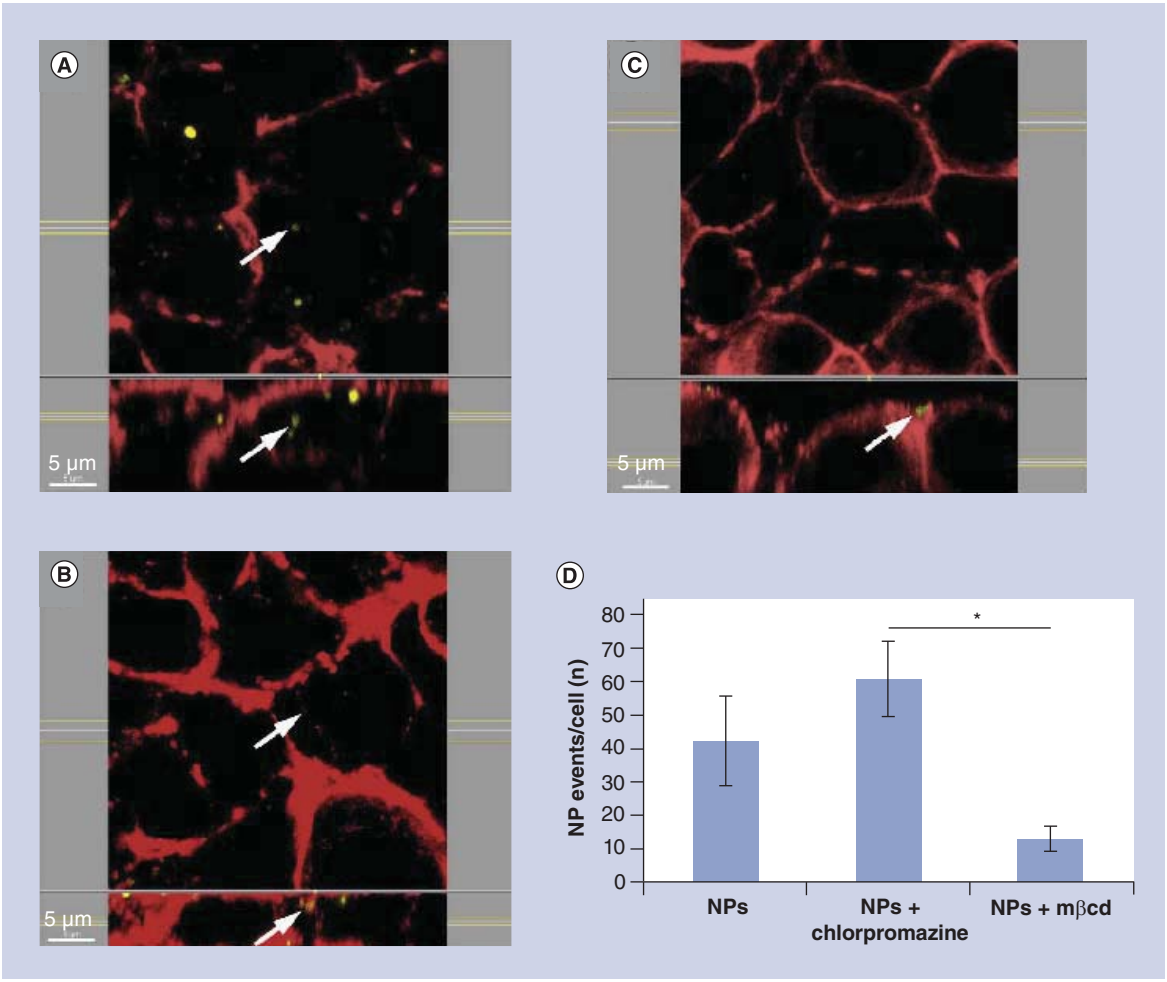

Figure 4. Particle uptake analyzed by means of laser scanning microscopy. (A–C) Representative fluorescent confocal micrographs show cellular NP uptake (NP: yellow; cytoskeleton: red). Intracellular NP events (white arrow) can be detected **(A)** within the cells of untreated cells and **(B)** cells incubated with chlorpromazine. As shown in **(C)**, cellular uptake was reduced after mβcd treatment. Quantitative evaluation of cellular NP uptake is shown in **(D)**, revealing a significant (*p > 0.05) decrease in NP uptake of mβcd- compared with chlorpromazine-treated cells. mβcd: Methyl-β-cyclodextrin; NP: Nanoparticle.

vesicles. We therefore conclude that these specific NPs enter the cells via endocytosis. This is in accordance with another study where differently coated Au NPs were mainly found in intracellular vesicles and only rarely in the cytosol. The Au NPs were not found in other intracellular compartments, such as the Golgi apparatus, endoplasmatic reticulum, nucleus or mitochondria [33]. However, coating of NPs with polyethylene glycol can significantly increase the particle number in the cytosol compared with uncoated particles [33]. In order to avoid any protein effects we used serum-free medium for the particle exposure.

The visualization of NP uptake by LSM and TEM and quantification suggest partial uptake of the polymer-coated Au NPs by caveolin-mediated endocytosis. The uptake of Au NPs via caveolin-mediated endocytosis has already been observed in previous studies [23,51,57,58]. These studies, however, used different models and differently modified and sized particles. For example, Hao and colleagues found a mβcd-mediated uptake inhibition of 10 nm cystein-cy5-coated Au NPs in HeLa cells [51]. The results of an *in vivo* study by Naota and colleagues showed localization of 20-nm plain, colloidal Au NPs in caveolin-1-positive stained vesicles in air–blood barrier cells in mice [58]. In a previous study with A549 cells and 15-nm sized plain and polyethylene glycol-coated Au NPs we found a mβcd-mediated inhibition after 1 h of 86 and 97%, respectively [33]. Particle-specific coatings therefore seem to determine cellular uptake mechanisms to a great extent. In the current study with polymer-coated Au NPs, only partial inhibition (63% inhibition) was achieved by mβcd. This suggests that

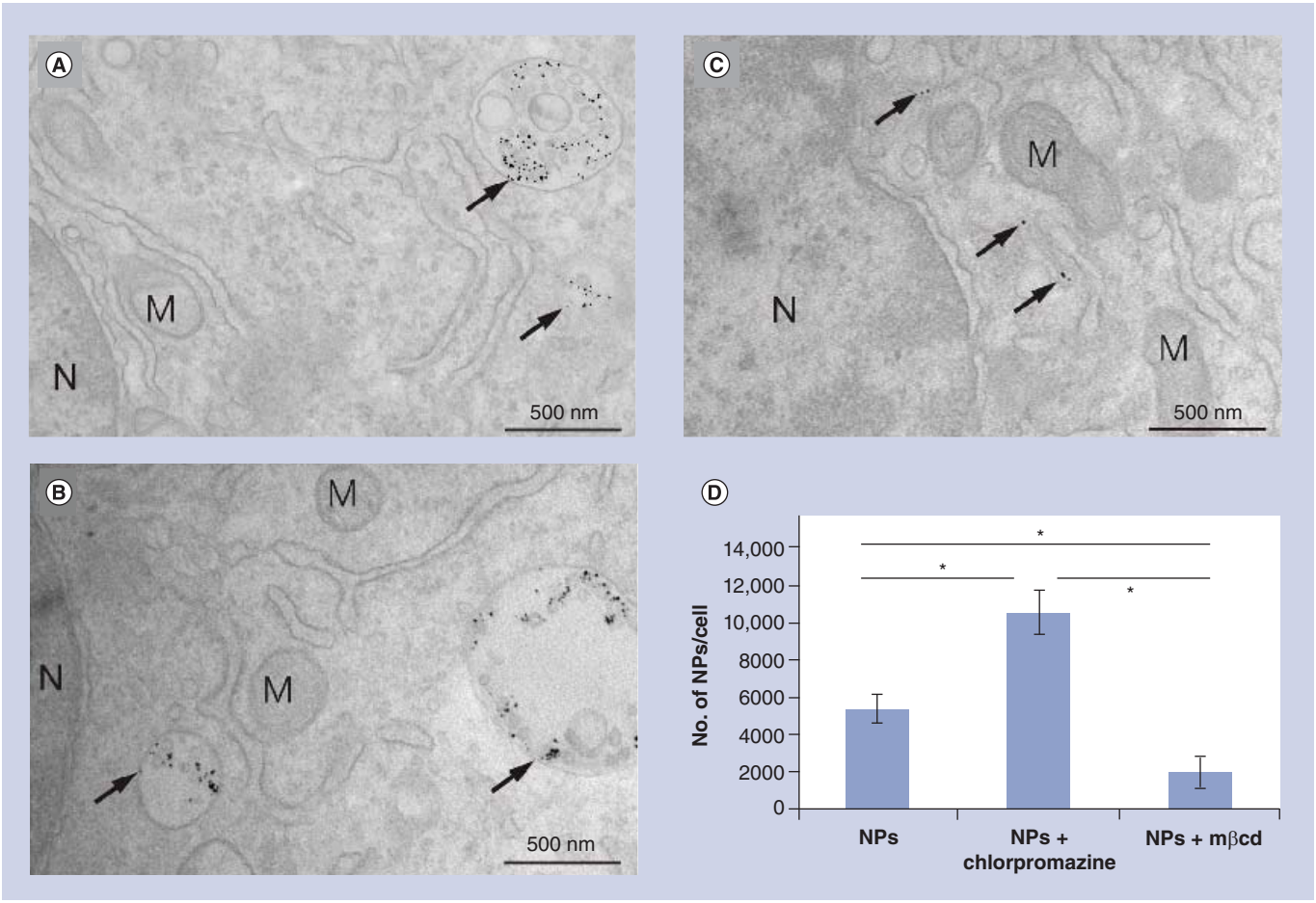

Figure 5. Nanoparticle uptake analyzed by means of transmission electron microscopy. **(A–C)** Intracellular NPs are shown in transmission electron micrographs. NPs (black arrow) can be detected within the **(A)** untreated cells and **(B)** cells incubated with chlorpromazine, as well as to a lesser extent in **(C)** mβcd-treated cells. NPs were all detected within some vesicular structures, but neither free in the cytosol nor within the nucleus or organelles such as mitochondria. A quantitative evaluation of the intracellular NP number is shown in **(D)**, revealing a significant (*p > 0.05) increase of intracellular NPs in chlorpromazine-treated cells and a decrease in mβcd-treated cells compared with the control.
M: Mitochondria; mβcd: Methyl-β-cyclodextrin; N: Nuclei; NP: Nanoparticle.

another prevalent mechanism could be involved such as macropinocytosis, clathrin-mediated endocytosis, or clathrin- and caveolin-independent endoytosis, as described previously [33]. However, we can exclude any NP uptake via clathrin-mediated endocytosis, since inhibition of this pathway did not decrease cellular NP uptake. On the contrary, chlorpromazine even induced a twofold increase of intracellular NPs compared with the control. This was observed by visualization and quantification methods via LSM and TEM. This increase was not expected because chlorpromazine was shown to efficiently inhibit the marker protein transferrin in the pre-experiments. In this case, we can further exclude any cellular NP entry due to disruption of the apical plasma membrane, since neither the LDH assay nor TEM images gave evidence of membrane distortion. Previous studies have shown that an inhibition of clathrin-mediated endocytocis can result in an increase in cellular macropinocytosis [59,60]. In accordance with our previous results that demonstrate that plain Au NPs stabilized with citrate enter A549 cells via macropinocytosis, it is very likely that the increase in intracellular NP number after inhibition of clathrin-mediated endocytosis results from enhanced macropinocytotic uptake. However, in other studies, NPs have often been described to be internalized via clathrin-mediated endocytosis [61,62] and chlorpromazine was shown to inhibit the uptake of fluorescein isothiocyanate–chitosan NPs in A549 cells [61]. The variety of different parameters, such as size, surface charge and coating or cell type, used in the different studies likely explain the different observations in the literature. This indicates that an adjusted experimental design is required, specifically when using different cell types, to learn more about the cellular mechanisms of NP interaction and uptake.

Stereological NP quantification via TEM & LSM

Both LSM and TEM analysis experiments were evaluated manually by means of stereology and a similar trend in the uptake ratio within experiments could be observed. An approximation of the incorporated amount of NPs per cell was determined by LSM combined with digital image restoration as previously described [9]. As indicated earlier, the resolution limit of light microscopy prevented us from distinguishing between single NPs observed with TEM and small NP agglomerates (events) observed with LSM. It is also well known that NPs inside cells are clustered in small vesicular structures and each vesicle can contain multiple NPs [48,63]. Therefore we counted 'NP events' in LSM, whereby one NP event likely corresponds to an individual vesicular structure that contains NPs. In this way we could quantify relative differences in the amount of incorporated NPs per cell under various uptake inhibitory conditions. Comparing the two approaches, we found approximately 150-times more NPs/cell in TEM than NP events/cell in LSM images. Note that TEM allows the individual resolution of intracellular NPs, whereas LSM does not. It has to be considered that NP characteristics, such as fluorescent intensity and wavelength, size, surface charge and tendency to form agglomerates, strongly affect particle resolution by LSM. The magnitude of the observed difference between the two techniques is therefore particle dependent and needs to be established individually for different NP types. It further has to be noted that more advanced LSM techniques in the category of super resolution laser microscopy such as stimulated emission depletion microscopy have recently become available. Thus, LSM resolution can be improved and LSM may become more appropriate for intracellular NP imaging [64].

Despite the limitation of single NP resolution by conventional LSM, the same trend in relative increase or decrease after endocytotic inhibition was observed with both techniques. There was a smaller divergence, however, between the mean values of the positive control and inhibition with chlorpromazine in the LSM results (30%) compared with the TEM results (50%). Therefore, the trend became more apparent in the results evaluated by TEM. Nevertheless, both methods showed an inhibition of NP uptake after mβcd treatment. Comparing the mean values of the positive control and inhibition with mβcd, the LSM results revealed a 96% distinction and TEM a 63% distinction. With the LSM approach, between 10 and 60 NP events were counted on average in control conditions in comparison to the individual NPs counted with the TEM method (mean: 5365 NPs). When visualizing the samples with TEM, it is also possible to detect single NPs and differentiate them from agglomerates, which, due to the optical resolution limit, is not possible with LSM. Another problem with LSM quantification is that fluorescent dyes might uncouple and separate from the gold cores. While strict purification made sure that only intact NPs were added to the cells, inside cells the polymer shell with the fluorophores may partially be removed from the NPs by intracellular degradation. At present, little is known about the integrity of NPs after incorporation by cells. When detecting the fluorescent signals, it is unfortunately not possible to determine whether or not the dyes are attached to the NPs. These problems also persist when the intracellular particle number is estimated by mean fluorescent intensity signal. Measuring cellular particle uptake via fluorescent intensity, such as by flow cytometry, is an easy and straightforward approach that has been used previously [65]. However, pitfalls such as intracellular signal quenching or uncoupling of fluorescent dyes remain and become more critical when particle types of different size, charge or fluorescent signals are compared with each other. In comparison, electron microscopy-based evaluations are certainly more labor intensive, but provide better resolution and allow the NPs to be assigned to the different intracellular compartments and quantify their relative intracellular localization [66]. Stereology is therefore the method of choice for quantifying cellular particle numbers in 3D from 2D microscopic images. Besides the approach

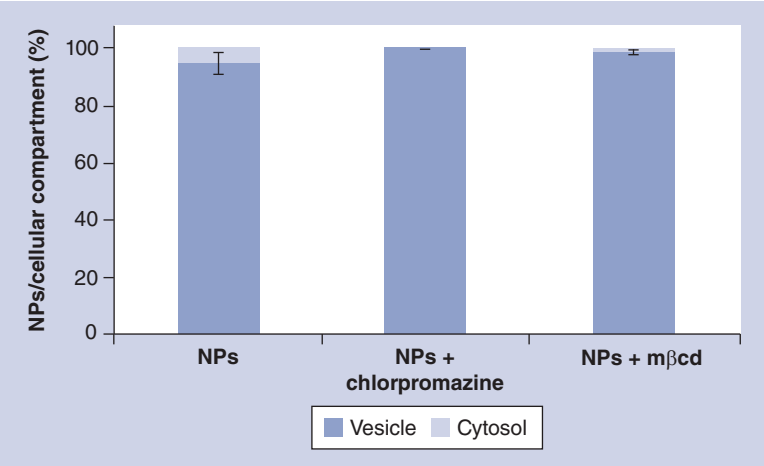

Figure 6. Intracellular nanoparticle distribution. The intracellular NP localization was acquired by random sampling and counting approximately 500–1000 NPs per sample (n = 3 for each experimental condition). The NPs were located in vesicles (95% or more) and no significant difference was found in intracellular localization after inhibition with chlorpromazine and mβcd.
mβcd: Methyl-β-cyclodextrin; NP: Nanoparticle.

described in this study and our previous study [33], another stereological design for quantifying cellular NP number by TEM has recently been proposed by Elsaesser and colleagues [37]. This approach uses the fractionator principle [67] and correlates the total amount of intracellular particles per sample with the total cell number per sample. The approach is easy to follow and well designed for convex cells in suspension. In the current study, however, we were using an adherent, alveolar epithelial cell line that was grown on an insert cell culture membrane. The application of the design presented by Elseasser and colleagues would therefore require an enzymatic digestion of the cells to detach them from the membrane. For this reason we preferred to use an approach that can be applied to any cell type and form and therefore allows quantification of intracellular NPs in an intact cellular monolayer. For further information on the differences between the two approaches we refer the reader elsewhere [68,69]. In comparison to our study, Shapero *et al.* analyzed the time-dependent uptake of particles quantified by flow cytometry and qualitatively analyzed by TEM and LSM microscopy [65]. Shah *et al.* used confocal Raman microscopy with a lateral resolution of 250 µm to quantify cellular particle uptake in correlation with fluorescence intensity [70]. However, this method cannot provide any spatial information about the NPs in a specific intracellular compartment. Due to the limited resolution of confocal Raman microscopy, atomic emission spectroscopy was applied to get an estimate of the signal-to-particle ratio. This is certainly valid information and in future studies the application of inductively coupled plasma-mass spectroscopy as a further internal control in combination with the stereological approach should be considered. However, compared with all these studies, this study is, to the best of our knowledge, the first to actually compare LSM with TEM resolution using a stereology-based approach and the same NPs for both microscopy methods.

Conclusion

In this study, two cutting-edge visualization and quantification methods (LSM and TEM) were used to analyze the endocytotic uptake mechanisms for polymer-coated Au NPs (hydrodynamic diameter: 21 nm) in A549 cells. Due to the fluorophore and the electron-dense properties of the NPs we were able to use the same cultures incubated with the particles and directly compare them. Although many inhibitors are described in the literature for the various uptake pathways, efficient inhibition was only achieved by 100 µM chlorpromazine for clathrin-mediated and 10 mM mβcd for caveolin-mediated endocytosis. Both inhibitors did not affect cell viability at the concentrations and incubation times used. Although we found in the literature many drugs that can be used to inhibit specific uptake pathways, only two out of the five inhibitors that we tested were effective and not cytotoxic. It is therefore indispensable to test for each cell type and each drug concentration the effectiveness of the inhibition by positive markers.

Furthermore, both visualization techniques revealed an inhibition of Au NP uptake with mβcd and thus revealed that caveolin-mediated endocytosis was the main uptake mechanism for the type of NP used in this study. In addition, we demonstrated that when using LSM only NP events and not the total numbers of NPs can be estimated. Furthermore, TEM analysis demonstrated that the estimated average Au NP number was in the range of several thousand per cell, and that more than 95% of the NPs were located in intracellular vesicles in the control as well as in drug-treated cells.

We have shown that the interactions of NPs with cells and quantification of NP uptake by cells can only be investigated under controlled experimental conditions and using cutting-edge microscopy techniques combined with stereological analysis.

Future perspective

The potential biomedical application of any NP requires a precise knowledge about the uptake mechanisms into any cell and the subsequent intracellular particle distribution. Until recently, most of the nanoresearch has been dedicated to providing a detailed description of the synthesis and characterization of NPs and their possible cellular reactions; however, in most of the experiments the characterization of the biological part is completely missing. Our results have clearly shown that biology should not be neglected and that, in our experience, inhibitors for endocytotic uptake pathways need to be tested and optimized. In addition, different methods should be used for the same end points and here we combined two stereological approaches based on light and electron microscopy. The limitations of each system needs, however, to be considered for the interpretation of the results. Unbiased stereology for quantitative image analysis will therefore be an important tool, since qualitative or semiquantitative investigations can lead to misinterpretation, especially in the field of NP–cell interactions. By understanding the underlying mechanism of the NP–cell interface we will have the possibility to design and optimize new nanotechnology approaches from basic research concepts to medical applications.

Acknowledgements

The authors would like to thank Andrea Stokes and Mohamed Ouanella for their excellent technical assistance and to Dr Jose Maria Montenegro Martos for helpful discussions.

Financial & competing interests disclosure

This study was supported by grants of the German Research Foundation (DFG, SPP 1313), the Swiss National Science Foundation and the Helmholtz Association. The authors have no other relevant affiliations or financial involvement with any organization or entity with a financial interest in or financial conflict with the subject matter or materials discussed in the manuscript apart from those disclosed.

No writing assistance was utilized in the production of this manuscript.

Ethical conduct of research

The authors state that they have obtained appropriate institutional review board approval or have followed the principles outlined in the Declaration of Helsinki for all human or animal experimental investigations. In addition, for investigations involving human subjects, informed consent has been obtained from the participants involved.

Executive summary

Inhibition of endocytotic mechanisms to study cellular nanoparticle uptake

- To reveal uptake mechanisms and intracellular detection as well as localization of any nanoparticle (NP), controlled biological conditions for the cells must be applied.
- The conditions for each endocytotic inhibitor (concentration as well as incubation time) have to be tested and optimized for each cell type used.

Quantification of NP uptake by stereology via laser scanning microscopy & transmission electron microscopy imaging

- By using hybrid gold NPs with a fluorescent and an electron-dense moiety the same particles can be used to evaluate different microscopic techniques such as laser scanning microscopy and transmission electron microscopy.
- Light microscopy techniques, such as laser scanning microscopy, allow only events and not total numbers of intracellular fluorescently labeled NPs to be evaluated.
- Transmission electron microscopy offers the advantage of providing spatial information on intracellular NP localization and allows, in combination with stereology, the determination of the total NP number/cell.
- Stereological analysis is the gold standard for quantitative analysis of microscopic data obtained by light or electron microscopy.

References

Papers of special note have been highlighted as: • of interest; •• of considerable interest

1 Joshi HM, Bhumkar DR, Joshi K, Pokharkar V, Sastry M. Gold nanoparticles as carriers for efficient transmucosal insulin delivery. *Langmuir* 22(1), 300–305 (2006).

2 You CC, Miranda OR, Gider B *et al.* Detection and identification of proteins using nanoparticle-fluorescent polymer 'chemical nose' sensors. *Nat. Nanotechnol.* 2(5), 318–323 (2007).

3 Jain PK, Huang X, El-Sayed IH, El-Sayed MA. Noble metals on the nanoscale: optical and photothermal properties and some applications in imaging, sensing, biology, and medicine. *Acc. Chem. Res.* 41(12), 1578–1586 (2008).

4 Verma A, Stellacci F. Effect of surface properties on nanoparticle–cell interactions. *Small* 6(1), 12–21 (2010).

5 Stark WJ. Nanoparticles in biological systems. *Angew. Chem. Int. Ed. Engl.* 50(6), 1242–1258 (2011).

6 Elsaesser A, Taylor A, de Yanes GS *et al.* Quantification of nanoparticle uptake by cells using microscopical and analytical techniques. *Nanomedicine (Lond.)* 5(9), 1447–1457 (2010).

• **Highlights the benefits and limitations of different analytical methods for intracellular nanoparticle (NP) quantification.**

7 Tantra R, Knight A. Cellular uptake and intracellular fate of engineered nanoparticles: a review on the application of imaging techniques. *Nanotoxicology* 5(3), 381–392 (2010).

8 Yu L, Andriola A. Quantitative gold nanoparticle analysis methods: a review. *Talanta* 82(3), 869–875 (2010).

9 Lehmann AD, Parak WJ, Zhang F *et al.* Fluorescent-magnetic hybrid nanoparticles induce a dose-dependent increase in proinflammatory response in lung cells *in vitro* correlated with intracellular localization. *Small* 6(6), 753–762 (2010).

10 Mühlfeld C, Rothen-Rutishauser B, Vanhecke D, Blank F, Gehr P, Ochs M. Visualization and quantitative analysis of nanoparticles in the respiratory tract by transmission electron microscopy. *Part. Fibre Toxicol.* 4, 11 (2007).

11 Lunov O, Syrovets T, Loos C *et al.* Differential uptake of functionalized polystyrene nanoparticles by human macrophages and a monocytic cell line. *ACS Nano* 5(3), 1657–1669 (2011).

12 Jiang X, Rocker C, Hafner M, Brandholt S, Dorlich RM, Nienhaus GU. Endo- and exocytosis of zwitterionic quantum

dot nanoparticles by live HeLa cells. *ACS Nano* 4(11), 6787–6797 (2010).

13 Sperling RA, Rivera GP, Zhang F, Zanella M, Parak WJ. Biological applications of gold nanoparticles. *Chem. Soc. Rev.* 37(9), 1896–1908 (2008).

14 Shukla R, Bansal V, Chaudhary M, Basu A, Bhonde RR, Sastry M. Biocompatibility of gold nanoparticles and their endocytotic fate inside the cellular compartment: a microscopic overview. *Langmuir* 21(23), 10644–10654 (2005).

15 Brandenberger C, Rothen-Rutishauser B, Mühlfeld C *et al.* Effects and uptake of gold nanoparticles deposited at the air–liquid interface of a human epithelial airway model. *Toxicol. Appl. Pharmacol.* 242(1), 56–65 (2010).

16 Peteiro-Cartelle J, Rodríguez-Pedreira M, Zhang F, Rivera Gil PR, del Mercato LL, Parak WP. One example on how colloidal nano- and microparticles could contribute to medicine. *Nanomedicine (Lond.)* 4(8), 967–979 (2009).

17 Dhar S, Reddy EM, Shiras A, Pokharkar V, Prasad BL. Natural gum reduced/stabilized gold nanoparticles for drug delivery formulations. *Chemistry* 14(33), 10244–10250 (2008).

18 Rosi NL, Giljohann DA, Thaxton CS, Lytton-Jean AKR, Han MS, Mirkin CA. Oligonucleotide-modified gold nanoparticles for intracellular gene regulation. *Science* 312(5776), 1027–1030 (2006).

19 Chen YH, Tsai CY, Huang PY *et al.* Methotrexate conjugated to gold nanoparticles inhibits tumor growth in a syngeneic lung tumor model. *Mol. Pharm.* 4(5), 713–722 (2007).

20 Rothen-Rutishauser B, Schuerch S, Gehr P. Interaction of particles with membranes. In: *The Toxicology of Particles.* Donaldson K, Borm P (Eds). CRC Press LCC, 139–160 (2007).

21 Unfried K, Albrecht C, Klotz LO, Von Mikecz A, Grether-Beck S, Schins RPF. Cellular responses to nanoparticles: target structures and mechanisms. *Nanotoxicology* 1(1), 52–71 (2007).

•• **Comprehensive review about the different uptake mechanisms of NPs and possible cellular responses.**

22 Hillaireau H, Couvreur P. Nanocarriers' entry into the cell: relevance to drug delivery. *Cell Mol. Life Sci.* 66(17), 2873–2896 (2009).

• **Review article on different cellular endocytotic mechanisms and their relevance for cellular NP uptake and drug delivery.**

23 Douglas KL, Piccirillo CA, Tabrizian M. Cell line-dependent internalization pathways and intracellular trafficking determine transfection efficiency of nanoparticle vectors. *Eur. J. Pharm. Biopharm.* 68(3), 676–687 (2008).

24 Chang J, Paillard A, Passirani C *et al.* Transferrin adsorption onto PLGA nanoparticles governs their interaction with biological systems from blood circulation to brain cancer cells. *Pharm. Res.* 29(6), 1495–1505 (2012).

25 Ruge CA, Kirch J, Cañadas O *et al.* Uptake of nanoparticles by alveolar macrophages is triggered by surfactant protein A. *Nanomedicine* 7(6), 690–693 (2011).

26 Ivanov AI. *Exocytosis and Endocytosis.* Department of Medicine, Gastroenterology and Hepatology Division, University of Rochester School of Medicine and Dentistry, Rochester, NY, USA, 15–36 (2008).

27 Perumal OP, Inapagolla R, Kannan S, Kannan RM. The effect of surface functionality on cellular trafficking of dendrimers. *Biomaterials* 29(24–25), 3469–3476 (2008).

28 Orlandi PA, Fishman PH. Filipin-dependent inhibition of cholera toxin: evidence for toxin internalization and activation through caveolae-like domains. *J. Cell Biol.* 141(4), 905–915 (1998).

29 Liu Y, Steiniger SC, Kim Y, Kaufmann GF, Felding-Habermann B, Janda KD. Mechanistic studies of a peptidic GRP78 ligand for cancer cell-specific drug delivery. *Mol. Pharm.* 4(3), 435–447 (2007).

30 Wang Z, Tiruppathi C, Minshall RD, Malik AB. Size and dynamics of caveolae studied using nanoparticles in living endothelial cells. *ACS Nano* 3(12), 4110–4116 (2009).

31 Puri V, Watanabe R, Singh RD *et al.* Clathrin-dependent and -independent internalization of plasma membrane sphingolipids initiates two Golgi targeting pathways. *J. Cell Biol.* 154(3), 535–547 (2001).

32 Rothen-Rutishauser BM, Kiama SG, Gehr P. A three-dimensional cellular model of the human respiratory tract to study the interaction with particles. *Am. J. Respir. Cell Mol. Biol. 32*(4), 281–289 (2005).

33 Brandenberger C, Mühlfeld C, Ali Z *et al.* Quantitative evaluation of cellular uptake and trafficking of plain and polyethylene glycol-coated gold nanoparticles. *Small* 6(15), 1669–1678 (2010).

• **Effect of NP coating and their subsequent uptake into epithelial cells assessed by means of stereology.**

34 Lin CA, Sperling RA, Li JK *et al.* Design of an amphiphilic polymer for nanoparticle coating and functionalization. *Small* 4(3), 334–341 (2008).

35 Zhang F, Ali Z, Amin F, Feltz A, Oheim M, Parak WJ. Ion and pH sensing with colloidal nanoparticles: influence of surface charge on sensing and colloidal properties. *ChemPhysChem* 11(3), 730–735 (2010).

36 Niebling T, Zhang F, Ali Z, Parak WJ, Heimbrodt W. Excitation dynamics in polymer-coated semiconductor quantum dots with integrated dye molecules: the role of reabsorption. *J. Appl. Phys.* 106(10), 104701–104706 (2009).

37 Elsaesser A, Barnes CA, McKerr G *et al.* Quantification of nanoparticle uptake by cells using an unbiased sampling method and electron microscopy. *Nanomedicine (Lond.)* 6(7), 1189–1198 (2011).

38 Shaw P. Deconvolution in 3-D optical microscopy. *Histochem. J.* 26(9), 687–694 (1994).

39 Stereo DC. The unbiased estimation of number and sizes of arbitrary particles using the disector. *J. Microsc.* 134(Pt 2), 127–136 (1984).

40 Small JV. Measurement of section thickness. In: *Abstracts of the Fourth European Conference on Electron Microscopy.* Rome, Italy, 609–610 (1968).

41 Jensen EBV, Gundersen HJG. The rotator (Vol 170, Pg 35, 1993). *J. Microsc.* 170, 282 (1993).

42 Dorph-Petersen KA, Nyengaard JR, Gundersen HJ. Tissue shrinkage and unbiased stereological estimation of particle number and size. *J. Microsc.* 204(Pt 3), 232–246 (2001).

•• **Examines the estimation of particle numbers by unbiased stereology.**

43 Rothen-Rutishauser B, Grass RN, Blank F *et al.* Direct combination of nanoparticle fabrication and exposure to lung cell cultures in a closed setup as a method to simulate accidental nanoparticle exposure of humans. *Environ. Sci. Technol.* 43(7), 2634–2640 (2009).

44 Rothen-Rutishauser B, Clift MJD, Jud C, Fink A, Wick P. Human epithelial cells *in vitro* – are they an advantageous tool to help understand the nanomaterial–biological barrier interaction? *Euro. Nano Tox. Lett.* 4(1), 1–20 (2012).

45 Dautry-Varsat A. Receptor-mediated endocytosis: the intracellular journey of transferrin and its receptor. *Biochimie* 68(3), 375–381 (1986).

46 Nabi IR, Le PU. Caveolae/raft-dependent endocytosis. *J. Cell Biol.* 161(4), 673–677 (2003).

47 Rodal SK, Skretting G, Garred O, Vilhardt F, van Deurs B, Sandvig K. Extraction of cholesterol with methyl-β-cyclodextrin perturbs formation of clathrin-coated endocytic vesicles. *Mol. Biol. Cell* 10(4), 961–974 (1999).

48 Brandenberger C, Clift MJ, Vanhecke D *et al.* Intracellular imaging of nanoparticles: is it an elemental mistake to believe what you see? *Part. Fibre Toxicol.* 7, 15 (2010).

49 Petri-Fink A, Rothen-Rutishauser B. Nanoparticles and cells: an interdisciplinary approach. *Chimia (Aarau)* 66(3), 104–109 (2012).

50 dos Santos T, Varela J, Lynch I, Salvati A, Dawson KA. Effects of transport inhibitors on the cellular uptake of carboxylated polystyrene nanoparticles in different cell lines. *PLoS ONE* 6(9), e24438 (2011).

51 Hao X, Wu J, Shan Y *et al.* Caveolae-mediated endocytosis of biocompatible gold nanoparticles in living Hela cells. *J. Phys. Condens. Matter* 24(16), 164207 (2012).

52 Karjalainen M, Kakkonen E, Upla P *et al.* A Raft-derived, Pak1-regulated entry participates in α2β1 integrin-dependent sorting to caveosomes. *Mol. Biol. Cell* 19(7), 2857–2869 (2008).

53 Macia E, Ehrlich M, Massol R, Boucrot E, Brunner C, Kirchhausen T. Dynasore, a cell-permeable inhibitor of dynamin. *Dev. Cell* 10(6), 839–850 (2006).

54 Schnitzer JE, Oh P, Pinney E, Allard J. Filipin-sensitive caveolae-mediated transport in endothelium: reduced transcytosis, scavenger endocytosis, and capillary permeability of select macromolecules. *J. Cell Biol.* 127(5), 1217–1232 (1994).

55 Andrews LD, Cohen AI. Freeze-fracture evidence for the presence of cholesterol in particle-free patches of basal disks and the plasma membrane of retinal rod outer segments of mice and frogs. *J. Cell Biol.* 81(1), 215–228 (1979).

56 Quirin K, Eschli B, Scheu I, Poort L, Kartenbeck J, Helenius A. Lymphocytic choriomeningitis virus uses a novel endocytic pathway for infectious entry via late endosomes. *Virology* 378(1), 21–33 (2008).

57 Chen LQ, Xiao SJ, Peng L *et al.* Aptamer-based silver nanoparticles used for intracellular protein imaging and single nanoparticle spectral analysis. *J. Phys. Chem. B* 114(10), 3655–3659 (2010).

58 Naota M, Shimada A, Morita T, Yamamoto Y, Inoue K, Takano H. Caveolae-mediated endocytosis of intratracheally instilled gold colloid nanoparticles at the air–blood barrier in mice. *Toxicol. Pathol.* 41(3), 487–496 (2013).

59 Harush-Frenkel O, Debotton N, Benita S, Altschuler Y. Targeting of nanoparticles to the clathrin-mediated endocytic pathway. *Biochem. Biophys. Res. Commun.* 353(1), 26–32 (2007).

60 Harush-Frenkel O, Rozentur E, Benita S, Altschuler Y. Surface charge of nanoparticles determines their endocytic and transcytotic pathway in polarized MDCK cells. *Biomacromolecules* 9(2), 435–443 (2008).

61 Huang M, Ma Z, Khor E, Lim LY. Uptake of FITC-chitosan nanoparticles by A549 cells. *Pharm. Res.* 19(10), 1488–1494 (2002).

62 Rejman J, Oberle V, Zuhorn IS, Hoekstra D. Size-dependent internalization of particles via the pathways of clathrin- and caveolae-mediated endocytosis. *Biochem. J.* 377(Pt 1), 159–169 (2004).

63 Parak WJ, Boudreau R, Le Gros M *et al.* Cell motility and metastatic potential studies based on quantum dot imaging of phagokinetic tracks. *Adv. Mater.* 14(12), 882–885 (2002).

64 Muller T, Schumann C, Kraegeloh A. STED microscopy and its applications: new insights into cellular processes on the nanoscale. *ChemPhysChem* 13(8), 1986–2000 (2012).

65 Shapero K, Fenaroli F, Lynch I, Cottell DC, Salvati A, Dawson KA. Time and space resolved uptake study of silica nanoparticles by human cells. *Mol. Biosyst.* 7(2), 371–378 (2011).

66 Mühlfeld C, Mayhew TM, Gehr P, Rothen-Rutishauser B. A novel quantitative method for analyzing the distributions of nanoparticles between different tissue and intracellular compartments. *J. Aerosol. Med.* 20(4), 395–407 (2007).

67 Gundersen HJ. The smooth fractionator. *J. Microsc.* 207(Pt 3), 191–210 (2002).

68 Howard CV, Elsaesser A. Letter to the Editor: Quantification of nanoparticle 'dose'. *Nanomedicine* 6(7), 1153–1154 (2011).

69 Mühlfeld C, Brandenberger C. Letter to the Editor: uptake of nanoparticles by cells: do you know their number? *Nanomedicine* 6(7), 1149–1151 (2011).

70 Shah NB, Dong J, Bischof JC. Cellular uptake and nanoscale localization of gold nanoparticles in cancer using label-free confocal Raman microscopy. *Mol. Pharm.* 8(1), 176–184 (2010).